IEEE Access
Multidisciplinary | Rapid Review | Open Access Journal

Received January 11, 2022, accepted February 24, 2022, date of publication March 4, 2022, date of current version March 15, 2022.

Digital Object Identifier 10.1109/ACCESS.2022.3156926

SF_6 Decomposed Component Analysis for Partial Discharge Diagnosis in GIS: A Review

AMMAR SALAH MAHDI, ZULKURNAIN ABDUL-MALEK, (Senior Member, IEEE), AND RAI NAVEED ARSHAD

Institute of High Voltage and High Current, School of Electrical Engineering, Faculty of Engineering, Universiti Teknologi Malaysia, Johor Bahru 81310, Malaysia

Corresponding author: Zulkurnain Abdul-Malek (zulkurnain@utm.my)

This work was supported in part by Universiti Teknologi Malaysia under Grant 05G88, Grant 4B482, and Grant 05G89.

ABSTRACT This paper compiles, summarizes, and deliberates over one hundred important works on the different approaches and advances in the surveillance and diagnosis of the internal status of SF_6 gas-insulated equipment (GIE), particularly partial discharge (PD) diagnosis in gas-insulated switchgear (GIS), and the proposed diagnosis techniques used. This review focused on four research aspects on PD diagnosis related to the SF_6 decomposition mechanism under PD activity, the developments in PD detection techniques, PD sources identification, and PD severity evaluation. Besides, the effect of various factors such as gas pressure, applied voltage, and impurities on the deterioration of the insulation gas and its influence on the diagnosis process has been reviewed. Currently, some reviews on PD diagnosis in SF_6-insulated switchgear have been presented and analysed; however, to date, most of them tend to focus on various PD detection techniques in GIS, while others are not extensive and comprehensive reviews. Unlike the available review publications, this paper highlighted various aspects of PD diagnosis in GIS and created a base for further development. The research trend in this field is expected to be directed toward a comprehensive assessment. This review provided a position of the current PD diagnosis in GIS studies and developments that can be a guideline for researchers for further research on the topic's actual impact in the field.

INDEX TERMS Decomposed component analysis, gas insulated switchgear, partial discharge, PD classification, PD detection, PD severity, SF_6.

I. INTRODUCTION

SF_6 gas is widely used as an electrical insulator in power systems due to its high dielectric properties and excellent arc quenching capability [1]. SF_6 has passed many qualification tests required for insulating gas in high voltage (HV) systems. It has become the most common insulation gas in modern high voltage, extra-high voltage, and ultrahigh voltage power system equipment [2]. These equipment include gas-insulated switchgear (GIS), gas-insulated transformer (GIT), and gas-insulated transmission line (GIL). Recently, the SF_6 market has expanded, with the electrical sector accounting for around 80% of total SF_6 demand [3]–[5]. Due to its wide usage in the power system, monitoring the performance of SF_6-insulated equipment is critical for a safe and reliable power system operation.

When subjected to electrical discharges, such as due to an electrical fault, portions of SF_6 gas dissociate or decompose into by-products, which in turn affect its overall insulation properties. Apart from electrical discharges, SF_6 decomposition may also be caused by thermal stress [6], [7]. Many researchers have studied the high current discharges, such as the arc and spark discharges, as well as the small current discharge or the partial discharge (PD), and the impact of the discharges on the insulation strength of the gas-insulated equipment (GIE) [8]–[11]. Various techniques were employed to detect the discharges, especially the partial discharge, including the acoustic, chemical, and ultrahigh frequency (UHF) techniques. There have also been significant attempts to apply different artificial intelligence (AI) approaches to recognise the PD sources and PD types, such as support vector machines (SVM) and wavelet transformations [12]–[14]. It is known that the PD pattern is a significant indicator to identify the type of PD source within a GIS [15]. In addition, it is also desired to be able to evaluate the degree of PD severity because this critical information can help in overall equipment condition monitoring. Previous research reported that the number of decomposed by-product

The associate editor coordinating the review of this manuscript and approving it for publication was Wei-Yen Hsu.

gases and their concentration could reflect the severity of PD activities in GIS [16], [17]. However, a specific guide for the PD severity evaluation is yet to be established [18]. In short, it is desired to have regular PD assessment of a GIE and early detection of possible insulation degradation may prevent catastrophic problems from occurring.

Recently, several techniques for monitoring and diagnosing GIS were proposed and developed. An illustration for these techniques, their working principle, and drawbacks are required. There are some review publications regarding these techniques available in the literature, which included trends and state of the art in particular aspects [19]–[21]. However, it does not comprehensively review developments in PD detection techniques, PD severity evaluation, and factors that cause SF_6 decomposition.

The motivation of this paper was to review recent monitoring and diagnosing development and trends toward a comprehensive evaluation of the SF_6 GIE, particularly GIS. By focusing on publications from the last decade, this review highlighted the causes of SF_6 deterioration, revealed PD detection methods, clarified various techniques used for PD and insulation defects identification, and provided a theoretical basis for current severity evaluation approaches. This review also presented a taxonomy for multiple strategies adopted in the literature and a starting point for further research on this topic, on top of identifying relevant gaps.

II. INSULATION CHARACTERISTICS AND DECOMPOSITION OF SF_6

SF_6 is a highly electronegative gas that attracts free electrons, resulting in a dielectric strength three times that of air at atmospheric pressure. It has good arc quenching properties and excellent insulation and heat transfer characteristics, making it an appropriate insulator in GIE. Pure SF_6 is an inert gas that is colourless, odourless, nontoxic, and noncombustible. Since it does not decompose at temperatures below 500 °C, pure SF_6 is heat-stable and has good thermal conductivity [7], [21]–[23].

It is known that SF_6 gas decomposes when subjected to an electrical discharge where the extent of the decomposition is related to the intensity or energy of the discharge [24], [25]. Previous investigations of SF_6 decomposition mechanisms under PD partial discharge were reported in [26] and [27]. To demonstrate the decomposition mechanisms under a negative corona, the authors proposed the case of a point-plane electrode configuration located in an SF_6 gas chamber. Three main regions were identified as the glow region, the ion drift region, and the main gas volume region as shown in Figure 1. In the glow region, SF_6 gas ionisation and dissociation are mainly caused by electron collision with SF_6 molecules. The ionisation process produces several low fluorine sulfides, namely, SF_5, SF_4, SF_3, SF_2, and SF. In addition, oxygen atoms (O) and hydroxides (OH) may also be produced by the dissociation of oxygen molecules (O_2) and water vapor (H_2O), respectively. Several additional components may be generated by the interaction of the above substances in the

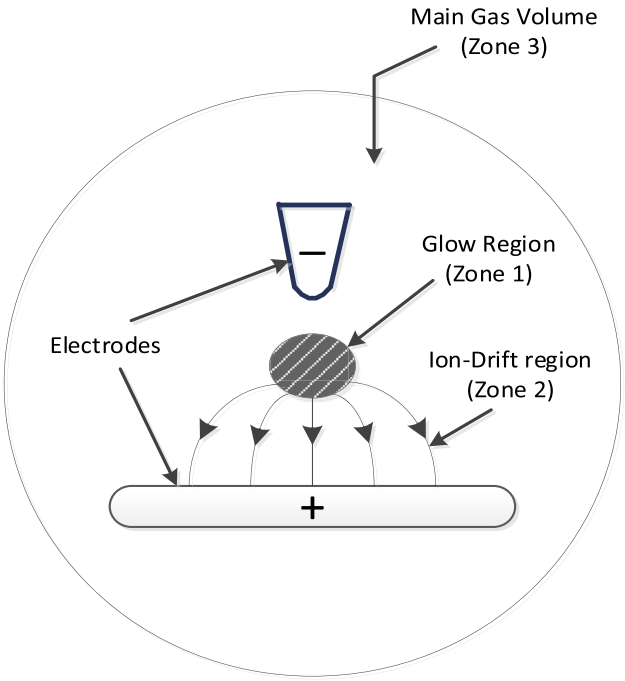

FIGURE 1. Three regions of the negative point-plane model of SF_6 decomposition [26].

glow region. These include long-lived gases such as sulphur dioxide (SO_2), thionyl fluoride (SOF_2), sulphuryl fluoride (SO_2F_2), and disulfur decafluoride (S_2F_{10}). Nevertheless, SF_6 molecules may also quickly reform due to self-healing process involving fluorine (F) atoms and low fluorine sulfides. Equations (1) to (12) illustrate the key reactions that occur in the glow area [26]–[28].

$$e + SF_6 \rightarrow SF_x + (6 - X)F + e, \quad X < 6 \tag{1}$$
$$e + O_2 \rightarrow O + O + e \tag{2}$$
$$e + H_2O \rightarrow O + OH + e \tag{3}$$
$$SF_5 + OH \rightarrow SOF_4 + HF \tag{4}$$
$$SF_5 + O \rightarrow SOF_4 + F \tag{5}$$
$$SF_4 + OH + F \rightarrow SOF_4 + HF \tag{6}$$
$$SF_3 + O \rightarrow SOF_2 + F \tag{7}$$
$$SF_3 + OH \rightarrow SOF_2 + HF \tag{8}$$
$$SF_2 + O \rightarrow SOF_2 \tag{9}$$
$$SF_2 + OH + F \rightarrow SOF_2 + HF \tag{10}$$
$$SF + O + F \rightarrow SOF_2 \tag{11}$$
$$SF + OH + 2F \rightarrow SOF_2 + 2HF \tag{12}$$

The ion drift region is located between the glow and the anode plane. In this region, negative ions are transported and then discharged at the anode. The volume encircling the point-plane area is the primary gas volume region. In this region, the chemistry is characterised by a slow gas-phase or surface reaction. As previously mentioned, in the glow region, the presence of SF_6 decomposition by-products and

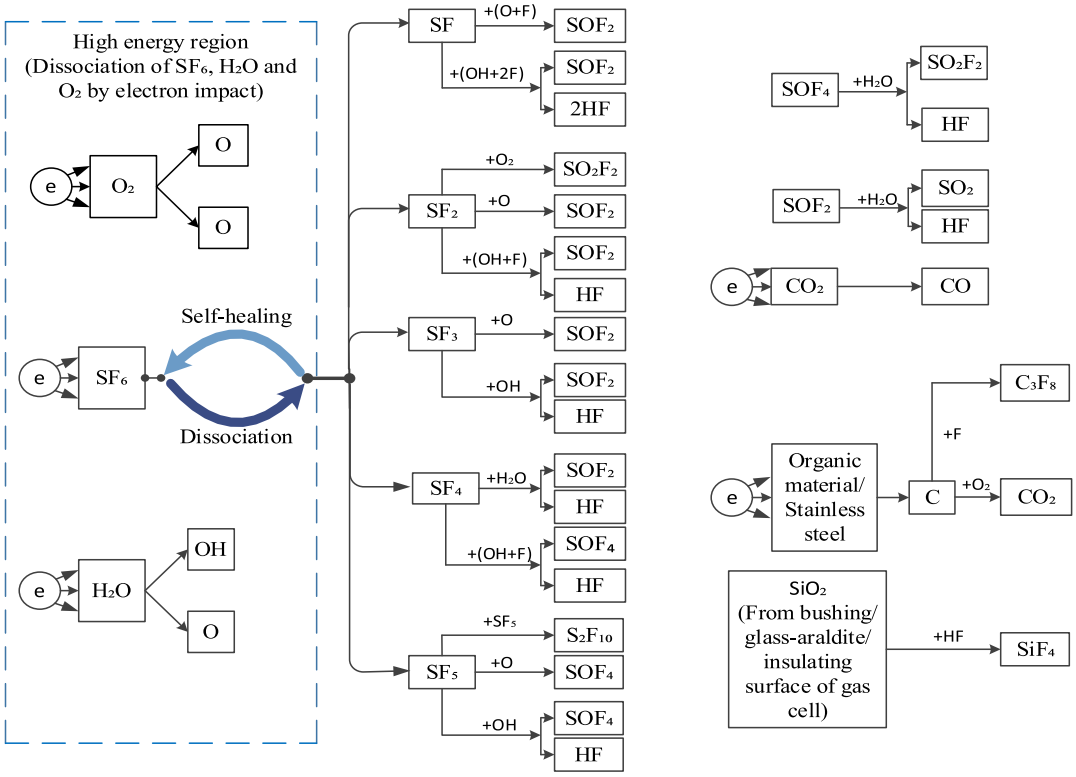

FIGURE 2. Formation of decomposition by-products under the activity of PD, including the formation of primary and long-lived products in the presence of impurities traces, solid insulator, and conductors.

other impurities, such as O_2 or H_2O molecules, leads to additional components to be produced. The additional components are produced due to further reactions in the main gas volume as described in (13) to (16).

$$SF_2 + O_2 \rightarrow SO_2F_2 \quad (13)$$

$$SF_4 + H_2O \rightarrow SOF_2 + 2HF \quad (14)$$

$$SOF_4 + H_2O \rightarrow SO_2F_2 + 2HF \quad (15)$$

$$SOF_2 + H_2O \rightarrow SO_2 + 2HF \quad (16)$$

Figure 2 summarises the formation of SF_6 decomposition by-products. More investigations on the decomposition mechanism and how to obtain decomposition characteristics under PD caused by various insulation defects are needed.

From the figure, the high-energy electron stream collides with SF_6 molecules under the influence of PD, resulting in gas decomposition into low fluorine sulfides. This collision splits S-F bonds, resulting in active F atoms and unstable SFx primary products [29]. Some reactions occur between these products and traces of H_2O and O_2, leading to multiple decomposition by-products.

In another research [30], a study was conducted to examine the behaviour of AC corona discharge on the decomposition mechanism. The author applied 50 Hz AC corona to a mixture of SF_6 gas and H_2O. Their findings showed that 50 Hz AC corona acted similarly to negative DC discharge.

III. MECHANISMS OF SF_6 DECOMPOSITION

Despite its excellent properties, SF_6 gas may decompose into various by-products as a result of an electrical discharge, as previously noted. Apart from electrical discharges, SF_6 gas may also decompose as a consequence of thermal overheat, also known as partial overheating fault (POF), and x-ray irradiation [6], [7]. The various SF_6 decomposition mechanisms are summarised in Figure 3. In the order of reducing energy, the electrical discharges can be further classified into arc, spark, and partial discharges [1], [31].

A. ARC DISCHARGES

Arc discharges are characterised by a current of a few thousands amperes, a discharge period from a few dozens to a few hundreds of milliseconds, an energy of about 10^5 - 10^7 J, and a temperature of up to 20,000 K [22], [32]. Power arc is generated during current interruption in circuit breakers, short circuits inside gas chambers, and disconnectors operation [33]. The SF_6 concentration in a GIS usually declines after an arc discharge.

The recovery of SF_6 after its decomposition is especially difficult due to the presence of impurities, such as water vapour and oxygen, as well as metal and carbon originating from electrodes and erosion [34]. Moreover, some newly generated decomposition by-products maybe corrosive, resulting in the corrosion of solid insulation materials and in a

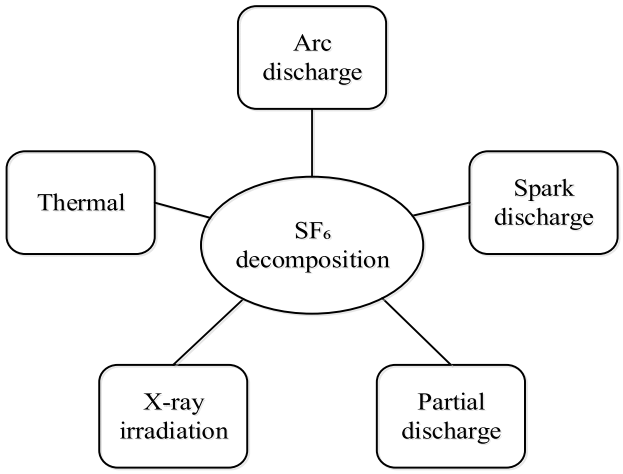

FIGURE 3. Various mechanisms of SF_6 decomposition.

reduction of the overall GIS dielectric strength. Other effects of arc discharge on the SF_6 decomposition mechanism in the presence of various impurities can be found in [34]. After an arc discharge, as the arc cools, sulfur and fluorine atoms may recombine to form SF_6 molecules. However, when the arc temperature drops from 12,000 K to 300 K, other by-products may also be generated [35], [36]. In a high-energy discharge, the SF_6 decomposition by-product is mainly SOF_2, as well as a small amount of SO_2F_2 [28], [31]. However, decomposition process is affected by impurities and materials included in the equipment.

Limited studies have been carried out to investigate the influence of some traces in SF_6 decomposition under arc discharge. In [37], the effects of trace H_2O and O_2 impurities and polytetrafluoroethylene (PTFE) vapour on SF_6 by-products were studied. Results obtained have found that the main products after arc quenching were CF_4 when PTFE was involved, SOF_2, SO_2 and $_2F_2$ when O_2 was involved, and SOF_2, SO_2 and HF when H_2O was involved. These findings emphasis the influence of various factors involved and its relevance to the decomposition process under arc discharge. Therefore, further studies to confirm the obtained results under various arc energies are needed.

B. SPARK DISCHARGES

Unlike an arc discharge, a spark discharge has a lower energy level, which is approximately 10^{-1} - 10^{2} J. It is noted that the discharge time affects the gas decomposition by-product's volume [22]. The spark's energy magnitude is three orders that of the corona [38], [39]. The sequence of electron avalanches that started at the cathode is crucial in spark discharge to create the gas breakdown [39]. Spark discharge is originated from higher field strength than the dielectric field strength of GIE, which is caused due to braking actions of disconnectors, fast transient overvoltage caused by ground faults, insulation defects inducing high local electric field strength, and continuous rising of equipment voltage [17]. Following a spark discharge, the organic insulation becomes carbonised by the high temperature spark, resulting in a decline in the overall dielectric strength and may pose a threat to the safety and stability of the power system operation, in addition to in extreme cases, the metal electrodes may be eradicated [38], [40].

Similar to other electrical discharges, a spark discharge may produce several SF_6 decomposition by-product gases. In a decreasing order of the quantity produced in a spark discharge, the by-product gases are SOF_2, SOF_4, SiF_4, SO_2F_2, and SO_2. Several other studies had also found S_2OF_{10}, $S_2O_2F_{10}$, and $S_2O_3F_6$ as by-products of a spark discharge in SF_6, and S_2F_{10} is regarded as the difference between spark discharge and PD or arc discharge despite its low content [31], [41]. Meanwhile, the decomposition process and generation of decomposition products under spark are affected by several factors, such as impurities traces of H_2O and O_2, gas pressure, solid insulating material and electrode material.

It is known that the gas pressure affects the accumulation of electron energy in a spark channel, causing electron intensity to be diverted into SF_6 [40]. However, in terms of the effect of gas pressure on the by-products produced by a spark discharge, the study found that it does not affect the types of generated by-products. Another investigation on the impact of H_2O on SF_6 dissociation under spark discharge was also performed [17]. Their results revealed that H_2O had a noticeable effect on the production rate of the decomposition by-products, namely, SOF_2, SO_2F_2, SOF_4, SO_2, and CF_4. On the other hand, O_2 greatly influenced the growth of SO_2F_2 and SOF_4 but not SOF_2 [38]. In general, previous studies have shown that impurities presence has a noticeable influence on the decomposition process, which determines the key feature parameters to recognize spark discharge in gas compartment. However, a diverse results of decomposition products and their content had been obtained, thus, further evaluation of the relation between various impurities content and generated products is essential for spark discharge diagnoses in GIS.

C. SF_6 DECOMPOSITION BY THERMAL EFFECT

Apart from the electrical discharge, the presence of heat can also cause the decomposition of SF_6 gas. For example, thermal decomposition of SF_6 occurs when a high current flow through an oxidised layer's contacts, which have high resistance and poor electrical conduction and hence overheating. Overheating can also be caused by other factors, such as electrical faults or short circuits caused by damaged insulation or current overload. Similar to the electrical discharge, thermally induced decomposition process produces several low fluorine sulfides, namely, SF_5, SF_4, SF_3, SF_2, and SF [5]. It is noted that thermal decomposition decomposes not only SF_6 but also the organic insulating materials such as the epoxy resin. As a result, H_2O molecules could be released and react with SF_6, this reaction develops the thermal decomposition of SF_6. In addition, the organic insulating materials attract F atoms from SF_6, resulting in low fluorine by-products [42]–[44]. In a decreasing order of the quantity produced in the thermally induced reaction, or partial overheating fault

(POF), are SO_2, SOF_2, SOF_4, SO_2F_2, and H_2S. SO_2 and SOF_2 account for 90% of SF_6 decomposition under the POF. Also, SO_2 is usually the first by-product produced, and its content increases with temperature [41], [45]. Nevertheless, the generated products and their content vary according to the temperature at the thermal fault location in GIS.

Previous researches have investigated the relationship between thermal fault temperature and the SF_6 decomposition process. An experimental study detected decomposition products under POF at a temperature lower than 400 °C [44]. Results showed that the most extensive products were SOF_2 and SO_2. The concentration of SOF_4 and SO_2F_2 was minimal, and H_2S was detected at temperatures above 340 °C. Furthermore, due to the above effect of organic insulating materials under overheating, decomposition of solid insulating materials has also been investigated under varied temperatures [42], [43]. Results had revealed that at 250°C, only H_2, CO, CO_2, and CH_4 can be detected. Whereas by rising temperature to 300°C, SOF_2, SO_2, H_2S, COS, and CF_4 have been detected. In brief, the above studies have shown that SF_6 thermal decomposition is closely related to the thermal fault temperature. However, the decomposition should consider not only direct thermal fault impact on SF_6, but also the presence of organic material, especially at various temperatures to propose consistent characteristics parameters for thermal fault in GIS.

D. SF_6 DECOMPOSITION BY X-RAY IRRADIATION

SF_6 gas can also be decomposed by x-ray irradiation. Similar to electrical discharge and thermal induced decomposition, SF_6 decomposes when exposed to x-ray irradiation. In certain applications, x-ray units are used in the vicinity of SF_6-insulated equipment for the purpose of equipment defect detection using digital imaging technology [46]–[48]. X-ray has been introduced as a defect detection technique due to its ability to penetrate and visually provide results for the internal status of GIS. The decomposition by-products produced by the exposure of x-ray are mainly similar to those produced under electrical discharges such as S_2F_{10} and SOF_2 [47].

The relative generation rates of S_2F_{10} and SOF_2 are approximately the same as in PD condition, however, S_2F_{10} generation rates are nearly a factor of ten less than that noticed for SOF_2 [47].

E. SF_6 DECOMPOSITION BY PARTIAL DISCHARGE

According to IEC 60270, partial discharge (PD) is defined as *a localized electrical discharge that only partially bridges the insulation between conductors and which may or may not occur adjacent to a conductor.* Insulating materials in high voltage electrical equipment can deteriorate chemically and physically as a result of PD activity. Being a type of partial discharge, the term corona discharge is used when the discharge occurs on the equipment's external surface. However, in GIS discharge monitoring, the terms PD and corona discharges are used synonymously [49].

In a GIS, PD is generated due to commonly found defects such as sharp protrusion tips on the current-carrying conductor or the metallic enclosure [24], [50]. When a sharp protrusion is present, its surrounding electric field may be distorted, leading to a strong local electric field. Hence local discharges can easily occur around such a sharp protrusion. A stable PD is initiated when the GIS is energised at standard operating voltage. A complete breakdown of the GIS may eventually occur after a certain period of continuous PD due to SF_6 gas degradation, or when the GIS is under an overvoltage. Consequently, due to the PD activity, the equipment's withstand voltage decreases considerably [51]. Untreated defects cause insulation deterioration to aggravate, and PD activity gradually leads to a severe spark fault. Apart from a sharp protrusion, other defects or sources of PD in GIS include free conducting particles, floating components, voids, and contaminations on the solid dielectric and on spacers used to support high voltage conductors [52], [53]. The free-moving non conducting particles may also become dangerous when mechanical vibration occurs due to the electrostatic force, and hence inducing PD by their movement [9].

In GIS, PD is considered an indicator of dielectric's degradation and the initial cause of the deterioration rate's acceleration. The types and concentrations of decomposition components are strongly affected by defect severity, applied voltage, discharge duration, and gas pressure [54]. Despite its low energy compared to arc and spark discharges, and its low discharge current in the order of microamps, PD represent 85% of causes of GIS catastrophic failures. When the PD occurs over a long period, many decomposition products are generated [20], [22]. For example, a corona discharge in SF_6 gas produces SO_2, CF_4, SOF_4, SO_2F_2, HF, SOF_2, and CS_2 [39]. Numerous previous studies were conducted to understand the decomposed components for better GIS monitoring. Nevertheless, PD diagnostic in GIS by studying SF_6 decomposition components is a research topic that still requires further investigation.

F. SUMMARY OF MAIN DECOMPOSITION PRODUCTS UNDER ELECTRICAL DISCHARGES

Various electrical discharges could cause an extensive dissociation of SF_6 into its lower sulfur fluorides. Further reactions of these sulfur fluorides with traces of residual moisture or oxygen lead to the generation of further by-products. The type of by-products and their generation rate vary according to the electrical discharge type. Table 1 summarises the main SF_6 decomposition by-products under main discharges based on the discharge energy. It is noted that each component's production rate varies according to the decomposition mechanism, making it a helpful tool to identify the internal deterioration type.

IV. PD DETECTION METHODS IN GIS

The GIS integrity and reliability are crucial to the overall safety and continuity of a power grid. As previously noted, partial discharges occur in a GIS even at the normal operating

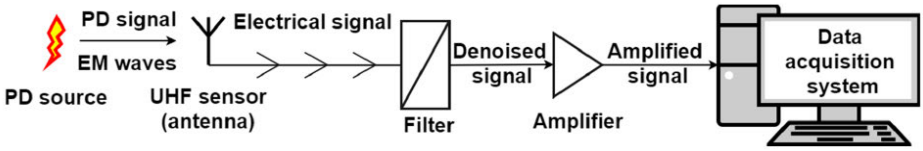

FIGURE 4. A block diagram of PD measurement using UHF [57].

TABLE 1. Main SF6 decomposition by-products production under main discharges.

Discharge type	Main SF_6 decomposition by-products	References
Arc	Mainly SOF_2 and a low amount of SO_2F_2	[31]
Spark	Mainly SOF_2, SO_2F_2, and SO_2. SO_2F_2 volume fraction is more than that produced by arc	[31] [39]
PD	Mainly SOF_2, SO_2F_2, SOF_4 and SO_2	[92][39]

voltage, and these discharges may eventually lead to the GIS failure. Hence, early detection and assessment of PD in a GIS is paramount. There are various methods available to detect the PD occurrence.

When a PD occurs, electromagnetic waves, high-frequency switching pulses, light, sound, and decomposition by-products, may all be accompanied, and serve as measurable quantities for PD detection and hence, insulation diagnostic [19], [55]. The available methods used to detect PD are categorized as either conventional, that is based on current or charge measurement as described in IEC60270 standard, or nonconventional, that is based on other quantities or physical phenomena such as electromagnetic waves, light, sound, and decomposition by-products [50], [52], [56], [57].

A. ELECTRICAL METHODS

The electrical PD detection is based on the detection of high-frequency current pulses, electromagnetic waves and apparent power loss that accompany the occurrence of PD. The pulse currents can be measured using a discharge free high voltage coupling capacitor in series with a low voltage arm (high pass filter), high-frequency current transformer (HFCT), or a Rogowski coil. The pulse current detection method is able to measure the apparent charge in pico Coulombs (pC). However, due to its low resistance to electromagnetic interference, it is inappropriate for online measurement [50], [58], [59].

In GIS, the electromagnetic wave generated by PD activity can induce a transient voltage on the cylindrical wall of the GIS, also known as transient earth voltage (TEV), which can then be measured using a capacitive probe or divider [60]. The TEV is formed on the metal surface in GIS due to high-frequency electromagnetic waves spreading across the insulator and flange junctions, representing discontinuities in GIS and allowing high-frequency PD to propagate to the outer metal. However, electromagnetic interference and peripheral noise could affect the PD detection using this method.

The HFCT is also employed for PD detection by clamping around cables and GIS case ground [19], [21]. As previously noted, PD detection using HFCT is based on the detection of PD pulses-induced currents. These currents mainly flow through the inner compartment part of GIS and the primary conductor's outer part. PD signals far from the PD source could also be measured using HFCT due to the lower attenuation of induced currents [61].

The electromagnetic waves generated by a PD activity can be conveniently measured using suitable antennas such as flat or horn shaped antennas. In a gas insulated switchgear (GIS), the antenna is in the form of a disc and is located at suitable places along the GIS cylinder, such as at the interfaces. These are also known as UHF sensors or disc couplers. The UHF detection range is mainly between 0.3 and 3.0 GHz [62]. The first stage in UHF PD measurement is to obtain electromagnetic signals for further signal processing. Hence, the accuracy and sensitivity of measures will be significantly influenced by UHF sensor characteristics and system configuration. Figure 4 shows a block diagram of UHF PD measurement [57].

The structure of UHF sensors varies according to the antenna applied for signals detection. In GIS, UHF antenna could be installed internally to the inner surface of the compartment, or externally which has been developed and utilised for PD monitoring. It includes windowed and barrier couplers installed at different locations [57], [62]. With the external installation, the integrity of the insulation system is less affected.

The UHF method has several advantages, including high sensitivity and good anti-interference capability [58]. However, the UHF approach is ineffective for detecting mechanical vibrations, which are basically based on acoustic pressure waves emitted due to the occurrence of PD [21]. It also has problem with discharge calibration, and low-energy discharges are challenging to notice [32], [50], [59], [63].

Another type of electrical method for PD detection is through the use of apparent power loss or loss tangent measurement. However, this measurement only gives the bulk characteristics of PD activities in the form of apparent power loss measured using Schering bridge. It is useful to determine conditions of equipment such as motors and generators.

Among the electrical detection methods, pulse current is the only one that could provide quantitative

determinations [60]. In short, the electric methods have the limitations of interference, sensitivity, and its ability for online detection.

B. ACOUSTIC METHODS

The resultant mechanical vibration and ultrasonic waves with long wavelengths, strong directionality, and concentrated power produced by PD and particle movement can be detected using acoustic sensors. GIS uses it to identify insulation defects by extracting parameters from detected acoustic signals by an appropriate acoustic sensor [64].

The most widely used acoustic sensor is the piezoelectric transducer. It includes a polarised material that serves as the active element. Mechanical vibrations will be converted to electrical signals by this sensor and vice versa [65]. Acoustic sensors are immune to electromagnetic interference, but low-energy discharges are not detected at the preliminary stage due to acoustic signal attenuation [32]. It is also easy to install on the equipment's surface [21]. However, noise can significantly affect ultrasonic detection, leading to inaccurate detection and identification of PDs [50], [59]. The precision of the acoustic and electrical methods heavily relies on an adequate signal-to-noise ratio [63].

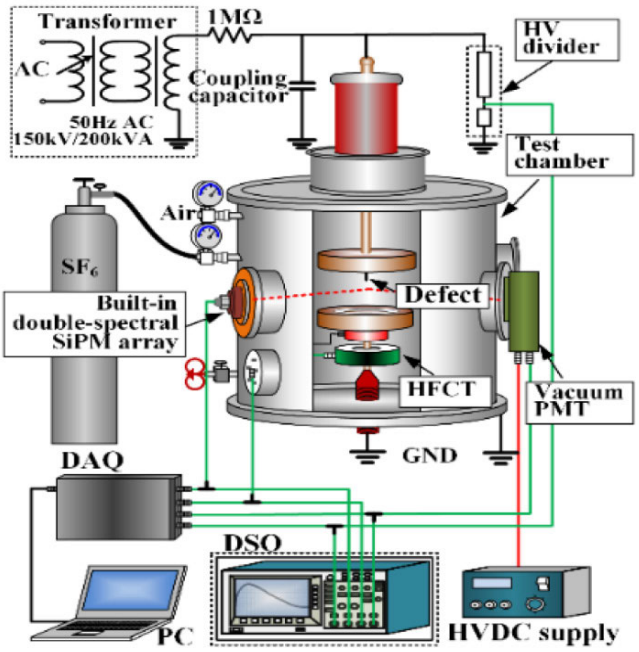

FIGURE 5. Schematic diagram of the synchronous PD measurement system [68].

C. OPTICAL METHODS

PD activity also produces light radiation from current flow, in addition to electromagnetic radiation, and acoustic waves [66]. The direct detection method of produced optical signals in GIS has gained growing interest. It has high sensitivity and immunity to electromagnetic interference (EMI) [67]. Sensors of this type have been installed in the GIS. As a result, this method is effective when the discharge source generates light. However, this method is invasive due to the need to mount the sensor into the GIS.

A vacuum photomultiplier tube (PMT) and a high-speed intensified charge-coupled device (ICCD) were used for optical PD measurement. However, their application was limited to laboratory studies and was hardly applicable to practical SF_6 insulated equipment. This drawback can be improved by employing a single-photon level photosensitive technique. On a millimetre scale, the silicon photomultiplier (SiPM) is a single-photon sensitive sensor made up of thousands of single-photon avalanche diodes (SPAD). Its competitive features include a low bias voltage, high quantum efficiency, and compact device size, making it a viable replacement for other photoelectric sensors such as PMTs [68], [69].

A double spectral SiPM sensor technique to diagnose PD in GIS was reported [68]. Figure 5 shows the schematic diagram of the synchronous PD measurement system. The results demonstrated that the SiPM sensor had the same sensitivity to PMT detection and HFCT. However, SiPM sensors required internal installation, and further confirmation is needed in real GIS. Furthermore, fluorescent optical fiber has been applied to detect PD in GIS and transformer [70]. In this technique, the optical signal is converted into an electrical signal using a photomultiplier tube. This method is less affected by EMI and was able to detect the optical signals of PD. However, the optical signal encounters an attenuation in transformer more than in GIS due to the nature of signal blocking, that is by the internal structure in the GIS and by windings in the transformers.

D. CHEMICAL METHODS

The chemical diagnostic technique which is known as decomposed component analysis (DCA) or chemical by-product analysis, has attracted the attention of researchers. This method is based on the analysis of SF_6 decomposition products generated by the PD activity. The presence of PD in GIS may decompose SF_6, resulting in various products with different concentrations. The type and concentration of the SF_6 decomposition components in GIS could provide sufficient information on the degree and type of internal degradation before breakdown. Researchers discovered an approximately linear relationship between PD energy and the amount of SF_6 decomposition products. Product types and quantities are related to H_2O and O content, discharge quality, electrode materials, and so on [21]. Examples of gaseous or solid products include SOF_4, SO_2F_2, SOF_2, S_2F_2, SF_2, S_2F_{10}, CF_4, CO_2, SF_4, S_2OF_{10}, H_2S, HF, SO_2, SiF_4, WF_6, and CUF_2 [71].

This method has a significant potential for PD early warning with high sensitivity and factuality. Noise and EMI have a rare effect on chemical analysis, making them a useful diagnostic tool for detecting PD. The procedure is noninvasive and can be performed online [7], [35], [50], [63].

Methods used to analyse SF_6 decomposition by-products are Fourier Transform Infrared Spectroscopy (FTIR), gas

chromatography (GC), detector tubes, and gas sensors [7], [71]. The accuracy of these techniques and their ability to detect decomposition products is essential for accurate PD detection using the chemical method.

1) GAS DETECTION METHODS

The detection techniques of SF_6 decomposition products provide the required data to implement the DCA method and PD diagnosis. These techniques can detect the concentration of decomposition products in parts per million (ppm) level. However, their accuracy and ability to detect the types of products are varied. The working principle, advantages, and drawbacks of the tools have been discussed.

a: DETECTOR TUBE

A detector tube is an analytical method that utilises chemical reactions in a test tube to identify the decomposition products [20]. Detector tubes are typically used for on-site detection, but large sample volumes and high cross-sensitivity defects make it difficult to detect gases correctly [64]. Certain decomposition products, such as SOF_2, SO_2, and HF, can only be observed when commercial detector tubes analyse SF_6 gas decomposition by-products. A detector tube's accuracy can even exceed μL/L. However, temperature and humidity do not affect its stability. Besides, cross-interference exists due to positive interference when some compounds are chemically similar to the target compound [7].

b: GC

GC is a gas analysis method that is based on column separation. The process begins by vaporising the sample mixture before a carrier gas such as nitrogen, hydrogen, or helium transports the sample through a chromatographic column. The flow of the sample with the carrier gas causes the samples' components separation. The separated components are then sent into a detector to record signals and transform them into a chromatograph. Components separation occurs at different times, which is referred to as the retention time [72]. Figure 6 shows a block diagram of the main parts of GC. The first part is the injector, through which the sample is introduced. The chromatography column is placed in the oven, while the detector provides the signal of separated components [73].

Although GC has excellent accuracy, it requires periodic maintenance; hence cannot continuously track the gas [63]. With precision, the GC system can detect most components, such as SO_2,SOF_2, SO_2F_2, and CF_4, which exceeds μL/L. Nevertheless, the sample injection time is exceptionally long, and the chromatographic columns require frequent cleaning. Therefore, this approach is unsuitable for online surveillance [7].

c: FTIR

The FTIR is the most widely used infrared spectrometer. It is based on infrared wavelength range measurements that the sample absorbs after being exposed to infrared radiation

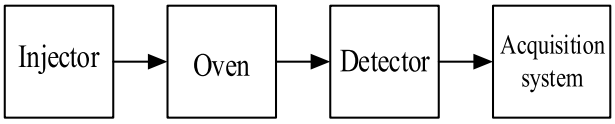

FIGURE 6. A block diagram of the main parts of GC.

from an infrared source. The presence of reference spectra is necessary for quantification [74], [75]. The FTIR detection technique has the advantages of being fast, could detect various component types, have high detection accuracy, resist disturbance, and identify the same sample repeatedly. Therefore, this technique is appropriate for online surveillance [7]. However, the dynamic configuration and high costs often hinder the practicality of FTIR and GC, making them more useful for offline laboratory research than on-site [63].

d: GAS SENSOR

An operation of a gas sensor is based on the conversion of measured gas concentration to an electrical quantity. The electrical properties of sensor materials can change due to the chemical properties of sensor material after it absorbs a gas molecule to its surface [76], [77]. The advantages of this gas-electric conversion sensor are its high-speed and performance. For SF_6 decomposition product detection, the gold(Au)-doped titanium dioxide (TiO_2) nanotube array sensor was proposed [78]. This study observed an improved gas sensing performance and reduced operating temperature for the TiO_2 nanotube array sensor. Phosphorene was also suggested to probe SF_6 decomposition gas sensors as it shows a variable response to SO_2, H_2S, and SF_6, revealing a promising material for online GIS diagnosis [79]. However, sensor poisoning occurs after prolonged use due to the chemical reaction between the sensor and the gases to be detected. Thus, the sensitivity and accuracy of the gas sensor could be affected [69], [79]–[81].

e: ULTRAVIOLET (UV) SPECTROSCOPY

UV detection is used in the 200 - 400 nm range of near UV light. The UV spectroscopy detection system consists of a fibre UV spectrometer, a deuterium lamp, transmitters, and a sample gas. Noninvasive measurements and a small scale in transformer diagnosis are among its advantages. However, UV absorption features of main by-products have not been observed, and the strict vacuum environment of detection restricts its applications. Thus, applying this technique for early on-site detection of PD is a topic worth investigating [63].

f: OVERVIEW OF GAS DETECTION TECHNIQUES

Electric gas sensors, FTIR spectroscopy, or GC may acquire more precise quantitative data. However, for on-site real-time monitoring, their practicability needs to be improved [63]. More research is required to develop a consistent detection system for detecting SF_6's decomposition under different

TABLE 2. Decomposition by-products detection techniques.

Detection method	Principle of work	Limitations	References
GC	Component's separation due to the different velocities in the separation column	Not suitable for online detection because of the complex structure and high cost, and cannot be used for continuous gas monitoring	[63][77]
Detector tube	Products identified by colour changes occurred due to chemical reactions in the test tube	In addition to the presence of cross-interference problems, temperature and humidity can easily affect its stability and are not suitable for on-site detection	[63][7][20]
Gas sensor	Chemical properties variations of gas-sensitive materials caused by the absorption of gas molecules by these materials	Detection accuracy may be affected because sensors poisoning occurs due to the reaction between gases to be measured and the sensor	[7][77]
UV spectroscopy	Products detection by selecting the suitable wavelength range	The primary by-products, such as SO_2F_2 and SOF_2, are not detected in the near UV region	[63]
FTIR	The infrared spectrum absorbed by a gas molecule	High cost and complex structure make it inappropriate for online monitoring	[63][20][7]

conditions. PD detection based on the chemical method using SF_6 decomposition by-products is a relatively new field. Various types of chemical analysis equipment have roughly different detection ranges for gases and their concentrations. Hence, more investigations using a chemical approach is required. Also, the relationship between generated gases and gas concentrations of decomposition by-products and the PD energy levels at various types, quantities, sizes, and materials of the defect must be reported. Table 2 summarises the decomposition by-products detection techniques.

2) PD ANALYSIS BASED ON DECOMPOSED COMPONENT ANALYSIS (DCA)

Decomposed component analysis has received attention as a promising diagnostic tool for GIE internal conditions. By qualitative and quantitative surveillance of the decomposition products, faults monitoring and the internal insulation condition can be realized, due to the close relation between generated products and their concentration with the type of insulation degradation [6]. Detecting the SF_6 decomposition products in the gas chamber refers to the presence of a PD source in the equipment [9]. The relationship between decomposition products and PD conditions has been investigated using the chemical detection method. For instance, in [54], the optical properties of the decomposition products have been evaluated using FTIR under different PD conditions. It is found that the content of CF_4, SOF_2, and SO_2F_2 has increased along the discharge period. The content of SO_2F_2 has increased with the increment of discharge voltage.

The process of PD analysis using the DCA method starts with the data collection using decomposition gas analysis tools such as FTIR and GC, and followed by the processing and selection of feature parameters; that could better improve the interpretation of PD activity. The selected characteristics features are then applied for AI techniques to monitor and diagnose PD activity within GIE. The characteristic decomposition products such as SOF_2 and SO_2F_2, products ratios such as SO_2F_2/SOF_2 and sulfur to carbon ratios, and the application of the artificial intelligence (AI) techniques such as SVM and tree-based algorithms are among the current PD data analysis techniques based on DCA method. Figure 7 shows the processes included in PD analysis using chemical analysis and AI techniques. Future studies on PD analysis using DCA are still needed due to limitations that are related to feature parameters extraction, selection of analysis techniques for source classification, and severity evaluation.

E. OVERVIEW OF PD DETECTION TECHNIQUES

Table 3 summarises the PD detection techniques while also revealing their limitations and working principles.

Table 3 shows that various GIS diagnostic techniques have detection range and physical quantity limitations. Indeed, these methods are capable of detecting PD in laboratory experiments. However, there are still shortcomings in field surveillance [19], [59], [63]. Moreover, none of these techniques can be utilised individually to eradicate the surrounding interference as the PD signals collected from each approach only include a specific facet of the information.

TABLE 3. Various approaches used for PD detection.

Detection method	Detection principle	Limitations	References
Pulse current method	Detection of pulse current that flows through coupling capacitors or ground wire, and measures discharge signal across external impedance	It has a low resistance capability to interference. Also, it is not suitable for online detection	[50][59] [19]
High-frequency current transducer (HFCT)	The technique utilises ferromagnetic cored induction coil to analyse and record PD transient signals	Interference signal produced from the ground wire may affect the detection results	[21][13]
TEV	Based on electromagnetic and radiofrequency radiation	Noisy environment and electromagnetic interference may affect PD detection	[85][70]
UHF	Detect electromagnetic waves produced by PD using a UHF sensor	The sensitivity and reliability of measured PD may be affected by external interference	[52][21]
Ultrasonic sensor	Detecting ultrasonic waves of mechanical vibration	Easily affected by noise, causing inaccurate PD measurement and recognition	[58][21]
Optical method	Detect the UV band of light emissions from PD	Detection is limited by the interference and sensors sensitivity	[19][55]
Chemical method	By detecting the SF_6 decomposition products produced by the activity of PD	Analysis of the decomposition components varies according to the used gas analysis technique	[28][93]

Recently, combined detection methods have been suggested by some researchers to improve the performance of diagnosing and monitoring systems while overcoming the limitations of a single approach [62], [82]. Consequently, effective diagnostic techniques are necessary to ensure high reliability in detecting defects that cause insulation deterioration. Figure 8 categorises the different methods for detecting PD in electrical equipment.

V. CLASSIFICATION METHODS OF PD SOURCES IN GAS INSULATED EQUIPMENT

Various AI techniques were used to intelligently classify PD defects in GIE when digital electronics and signal processing methods evolved. Significant efforts have been made to employ AI techniques such as artificial neural networks (ANN), wavelet transformation, and support vector machine (SVM) to classify PD sources automatically. PD classification in GIE have been reviewed based on studies employing both nonchemical and chemical analysis.

A. NON DCA-BASED CLASSIFICATION

This classification approach uses techniques such as the PD measurements, PD phase resolution (PRPD) pattern and X-ray irradiation to identify the types of defects in GIE.

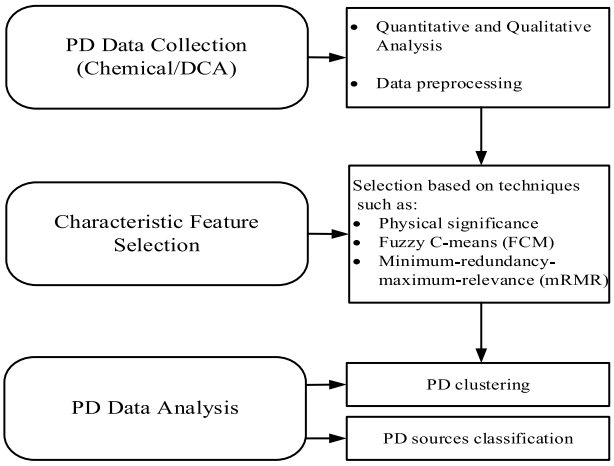

FIGURE 7. Block diagram of three components in partial discharge analysis based on chemical detection and artificial intelligence techniques.

X-ray digital imaging technology was applied to detect various defects: metal and flaky particles, Loosened Metal Screws, and different adsorbent cover materials [46]. The investigation concluded that the technique for visually detecting defects in GIS was effective. However, SF_6 may

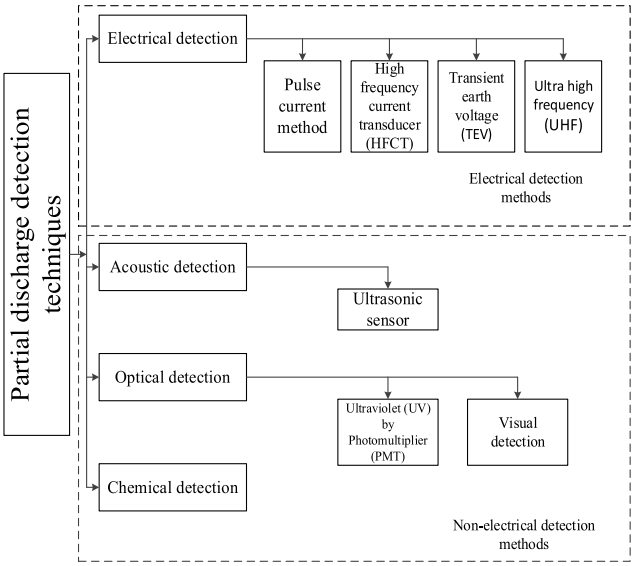

FIGURE 8. Various conventional and nonconventional PD detection techniques.

decompose due to X-ray irradiation by employing this technique, resulting in a significant reduction in SF_6 insulation. Consequently, more research is required to investigate the influence of X-ray on SF_6 gas before it can be applied on-site.

Moreover, a probabilistic neural network (PNN) was developed to classify PD produced by a floating electrode, polluted bushing, and free metallic particles in gas-insulated load break switches (GILBS). As for data reduction, the fuzzy C-mean method was employed [15]. Multisource PD classification was conducted by [83] using two-level logistic regression, with the feature extraction of PD signals was based on PRPD. The author revealed that a single class SVM could classify individuals based on multisource signals.

These methods have performed well; however, the accuracy of PD measurements was subjected to measurement and sensing devices ability [19], [84], [85]. Methods used to measure PD have limitations due to interference and noise accompanied by PD signals. Consequently, using noise removal techniques for better pattern recognition are required. Also, feature extraction of pertinent data from raw data is needed during the preprocessing stage.

Alternatively, chemical by-products might be considered by using SF_6 by-product concentration and ratios as feature characteristics to overcome the limitations of PD measured quantities.

B. DCA-BASED CLASSIFICATION

The concentration and concentration ratio of SF_6 decomposition products were used as feature parameters to classify insulation defects in GIE. A decision tree algorithm with concentration ratios as a classification parameter was suggested to detect GIS defects. A protrusion, free conducting particles, contamination, and gap were used as artificial defects for PD initiation [50]. However, decision tree faces the challenge of overfitting. Another author has used PSO-optimised SVM to discriminate four defects within a GIS, namely protrusion, particle, contamination, and gap defects. The author proposed three concentration ratios as a feature parameter for classification [52]. However, SVM performance was mainly dependent on algorithm parameters that the user must specify. The results have shown that the proposed method using the SVM and SF_6 decomposition by-products was able to successfully classify the defects to an accuracy up to 97.72 %.

Meanwhile, the backpropagation neural network (BPNN) algorithm was used to diagnose DC-GIE using feature sets of SF_6 decomposition quantities [16]. The authors compared the accuracy rate of identifying four types of defects (protrusion, free conducting particles, polluted insulation surface, and insulator gap) using concentration and its ratio from the suggested feature sets. Results found that the classification showed a high accuracy rate with the concentration ratio feature set. However, BPNN has a drawback related to overfitting if not generalised.

Meanwhile, SF_6 decomposition under three categories of PD sources was studied [86]. In the research, the random forest algorithm was employed. The outcome demonstrated a high classification accuracy compared to eight algorithms used to classify various defects utilising product concentration as a characteristic quantity. Based on the Duval idea used in the dissolved gas analysis (DGA) in transformers, the authors in [41] and [6] applied the triangle method to identify PD, POF, and spark fault in GIE. The concentrations of four decomposition products were selected to identify the three fault types to build the triangle sides. They found that a high accuracy rate was detected in the internal fault recognition using the diagnostic method. The researchers also concluded that it is possible to provide an on-site diagnosis for power equipment.

The triangle method with the decomposition product concentration and concentration ratios was also used for discharge recognition caused by the metal protrusion, floating, and insulator defects [87]. This graphical method had demonstrated reliability and sensitivity in recognising incipient faults. However, further confirmation is needed in real GIS.

Furthermore, the feasibility of recognising protrusion, particle, contamination, and gap defects using decomposition characteristics was investigated by [28]. After analysing the decomposition products, the author concluded that the four types of defects differ significantly in decomposition amount, decomposition rate, and concentration ratio. However, this classification depended on the user's knowledge of the decomposition product characteristics at each type of defect. A diagnosing method that combines two detection techniques for PD was proposed by [59]. The author used the UHF method for online detection while chemical analysis for offline detection. The obtained data with the Dempster-Shafer (DS) evidence theory application was used to classify four types of GIS defects. The results obtained using this combined method showed an improvement in diagnosing accuracy.

TABLE 4. Summary of defects recognition methods in GIE using chemical analysis.

Method	Characteristics features	Defect type	Limitation	Reference
Decision tree	Concentration ratios	Protrusion, free conducting particles, contamination, and gap	The challenge of overfitting and misclassification due to data outside limited value	[50][6]
SVM optimised by PSO	Concentration ratios	Protrusion, particle, contamination, and gap	An algorithm parameter setting is required. Also, it is a binary classifier	[52]
BPNN	Concentration ratios	Protrusion, free conducting particles, polluted insulation surface, and insulator gap	The drawback of overfitting if not generalised	[16]
Triangle method	Products concentration and concentration ratio	Protrusion defect, floating potential defect and insulator defect	Further confirmation is required in real GIS	[87]
The characteristics of decomposition	Analysing the decomposition products	Protrusion, particle, contamination, and gap	It depends on the user's knowledge of the decomposition products characteristics at each type of defect	[28]
Joint method of Chemical detection and UHF	concentration ratios and PD spectrum data	Protrusion, free metallic particle, contamination on spacers, and the gap at electrode/epoxy interface	Further confirmation is required in real GIS	[59]

There is still a need to test the method's performance in the gas chamber with simultaneous PD sources. Furthermore, more investigation of other combined detection techniques is required to compare performance with the proposed method. Table 4 illustrates some of the methods used to identify defects in GIE using chemical analysis, as well as its limitations

Previous works had been successful in detecting defects within GIS to some extent. However, applying AI techniques for PD source classification faces challenges in selecting appropriate features and a suitable classification algorithm, especially in multiple PD sources.

VI. DECOMPOSED COMPONENT ANALYSIS-BASED PD SEVERITY EVALUATION

An insulation status assessment includes determining the internal deterioration type and its severity [88]. Hence, the degree of severity has attracted researchers' interest based on the essential information obtained. Studies on PD severity have been conducted across single and multiple types of defects. However, most of these studies have focused on PD severity induced by the protrusion defect, which is a common and harmful defect in GIS. The protrusion has been simulated using a needle plane and point plane electrodes. The use of characteristics parameters extracted from experimental and theoretical studies to identify the internal operation condition in GIS can also be employed to evaluate the severity of the discharge [51]. Previous studies have found that the decomposition products' quantity, concentration, and ageing time variation can reflect the severity of PD in GIE [16], [17]. However, the criterion for PD severity evaluation has not yet been unified [18].

Several approaches have been investigated to evaluate the severity of PD. For instance, as decomposition occurs, SOF_2 and SO_2F_2 are generated [Equations (13) and (14)] due to the reaction of SF_4 and SF_2 with H_2O and O_2, respectively. Since the energy required to generate SF_2 is more than the energy needed to produce SF_4 to break the S-F bonds in the SF_6 molecule, SO_2F_2 content generated at a higher PD level is more significant than SOF_2. Thus, the ratio $(SOF_2+SO_2)/SO_2F_2$ can be used as a severity indicator. In such a way, the generation of decomposed components will define the PD's severity in GIE [89].

The results indicated that SO_2 concentration increases with PD improvement, whereas H_2S became a significant product that only generates high-energy discharges. Therefore, these two products can characterise insulation deterioration severity [29], [63], [90]. Besides, since the generation

TABLE 5. PD severity evaluation methods in GIS.

Method	Detection device	PD mechanism	Source of PD	Summary of findings	Reference
The ratio (SOF_2 + SO_2)/SO_2F_2	GC-MS	Corona discharge	Point-plane	The ratio of (SOF_2 +SO_2)/SO_2F_2 decreases with voltage increasing, and increases with SF_6 pressure increasing.	[89]
Effective energy characteristic ratio of (SO_2F_2)/(SOF_2)	GC	PD	Needle-plate electrode	Effective characteristics energy ratio proposed based on the ratio (SO_2F_2)/(SOF_2), the higher the ratio is, the larger the PD energy is.	[29]
PDAV and PDIV	GC-MS	PD	Point-plane electrode	Generation rate of SO_2F_2, SOF_2 + SO_2, increases with the rise of PDAV, while decreases with the increasing of PDIV	[51]
Three levels of PD based on PD quantities and decomposition products	GC-MS	Negative DC PD	Needle-plate electrode	PD status is evaluated based on its association with the generation and concentration of CF_4, CO_2, SO_2F_2, SOF_2, and SO_2)	[24]
Three levels of PD based on products concentrations	GC-MS	Negative DC PD	Free metal particle	Using DCA method shows good performance to diagnose PD severity	[88]
Effective generation rate	GC/GC-MS	Positive DC and AC PD	Protrusion, Particle, Contamination and gap	Under positive DC, the order of defects based on the effective generation rate of SO_2F_2, SOF_2, and SO_2 is protrusion > particles > contamination > gap. While under AC, the order is protrusion > contamination > particles > gap	[10]

rate of decomposed components was associated with the severity of discharge [91], it can assess the severity of the defect. For statistical representation, the effective generation rate was considered [10]. Another study also reported using the enhanced concentration ratio (SO_2F_2)/(SOF_2) by using the effective characteristic ratio to identify the PD energy statistically [29].

Furthermore, in another study, the changing levels of nonuniform field distribution distortion and PD magnitude were used in PD applied voltage (PDAV) and PD inception voltage (PDIV) to evaluate the severity of PD. The ratio (SO_2F_2)/(SOF_2+ SO_2) was applied as a criterion to specify the level of PD [51]. Meanwhile, characterising PD severity by using the average magnitude of PD was proposed by [88]. There were three levels assigned for PD severity, namely, mild, medium, and dangerous. The product growth had been correlated with the severity of PD at each level. Meanwhile, the BPNN and SVM algorithms were selected to diagnose it. Hence, it can be concluded that selecting concentration ratios as a feature parameter had shown higher accuracy than the concentration alone to diagnose the PD's severity.

A study [24] used the fuzzy C-means (FCM) algorithm to divide the PD into three levels based on the applied voltage, namely slight, medium, and severe, by using seven characteristic quantities of PD as feature parameters before correlating the SF_6 by-products at each severity level. A decision tree algorithm was then applied to obtain the PD status membership function value. A fuzzy comprehensive evaluation theory was finally used to assess the PD status. Previous studies have looked at the concentration of characteristic gases, which varies depending on the SF_6 decomposition process. Generally, studies on the severity evaluation criteria are required, and the severity of PD under different configurations of insulation defects needs additional investigation. Therefore, Table 5 summarises the techniques used to evaluate PD severity in GIS.

TABLE 6. Previous studies devoted to diagnosing SF6 insulated equipment by chemical analysis.

PD Mechanism	Detection device	Types of defects	Analysed products	Key findings	References
PD	GC	Needle-plate	CO_2, SOF_2, SO_2F_2, SO_2	The ratio of (SOF_2 + SO_2) and SO_2F_2 varies with the change of gas pressure and applied voltage	[94]
AC Corona	GC	Needle-plane	SO_2F_2, SO_2, and S_2OF_{10}	The average discharge capacity and its fluctuation tend to decrease as the moisture content increases	[95]
AC corona	GC	Point-plane	SOF_2, SO_2F_2, SO_2, CO_2	As the pressure increases, the concentration of SOF_2, SO_2F_2, SO_2, and CO_2 decrease	[96]
AC corona	GC	Needle-plane	SO_2F_2, SOF_2, CO_2, and CF_4	Concentration ratios of (SO_2F_2)/(SOF_2), (CF_4)/(CO_2) and (CF_4 + CO_2)/(SO_2F_2 + SOF_2) decrease with the increase of oxygen and moisture	[97]
AC PD	GC-MS	Point-plane	SO_2F_2 and SO_2	SO_2F_2 generation depend on O_2 and H_2O as well, while SO_2 has little dependence on O_2	[98]
AC PD	N/A	Needle-needle	SO_2, SOF_2, H_2S, CF_4, SO_2F_2, C_3F_8	At low energy discharge, SF_6 decomposition products concentration increase with the increase of discharge capacity	[99]
AC PD	FTIR		CF_4, SOF_2, and SO_2F_2	The content of SOF_2, CF_4, and SO_2F_2 increase with the increase of stress duration. By increasing voltage, SO_2F_2 increases while it decreases when the gas pressure increases	[54]
AC PD	GC-MS	Epoxy resin rod attached with copper powder	CS_2, SO_2, and COS	Carbonyl sulphide (COS) has generated when there is high PD intensity, which is produced near the occurrence of flashover	[100]
PD	GC	Needle-plane, Ball-plane, Plane-plane	CF_4, SO_2F_2, CS_2, SO_2, and S_2OF_{10}	CF_4, SO_2F_2, CS_2, SO_2, and S_2OF_{10} are generated under the normal operating of SF_6 insulated current transformer (CT)	[11]
AC PD	GC	Needle-plate	CF_4, CO_2, SO_2F_2, and SOF_2	H_2O prevents self-healing of SF_6 by capturing F atoms and causing SO_2F_2 to increase with its increment, while SOF_2 does not show a linear relation to H_2O	[101]
AC PD	GC, GC-MS, FTIR	Free conducting particle	CO_2, SOF_2, SOF_4, SO_2F_2, SO_2, SiF_4, S_2F_{10}, and CF_4	PD strength has a positive relation of a different degree with the formation of decomposition products	[102]
AC PD	GC	Needle-plate	CO_2, SO_2F_2, and SOF_2	The concentration of CO_2 and SOF_2 is not influenced by O_2, while O_2 negatively affects SO_2F_2 concentration	[93]
AC corona	GC-MS	Point-plane	SOF_2, SO_2, SO_2F_2, CF_4, and CO_2,	It is suggested that the ratio of (SOF_2 + SO_2) to SO_2F_2 is more affected by corona inception voltage more than that of the applied voltage	[103]
AC PD	GC	Needle-plate	CF_4, CO_2, SO_2F_2, and SOF_2	The characteristic energy ratio can reveal the PD energy	[25]
Negative DC PD	GC	Needle-plate	SO_2F_2, SOF_2, and SO_2	Generated products are significantly correlated with the type of defect material in the order Al > 304 stainless steel > Cu	[104]
Negative DC PD	GC-MS	Needle-plate	CO_2, SO_2F_2, SOF_2, SO_2, and CF_4	The concentration of decomposition products increases with the decrease of gas pressure	[105]

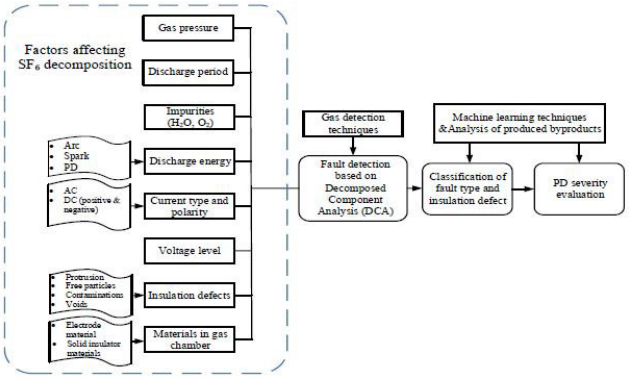

FIGURE 9. A comprehensive evaluation of GIS condition and fault detection using decomposed component analysis (DCA) consisting of consideration for various factors affecting SF_6 decomposition, decomposition by-products detection techniques, PD sources classification, and PD severity level evaluation.

VII. DISCUSSION

This study has presented significant drawbacks in the analysis of PD activity in GIE, which are related to PD detection, features parameters selection, and PD data analysis. The following section presents the various factors that could affect the SF_6 decomposition process, and hence the PD diagnosis in general.

A. COMPREHENSIVE DCA-BASED PD DIAGNOSIS CONSIDERING THE INFLUENTIAL FACTORS ON SF_6 DECOMPOSITION

Evaluating the internal status of SF_6-insulated equipment has been investigated previously under different conditions. Most of the results obtained were limited in discussing a specific facet that might affect SF_6 decomposition such as flaws and impurities. However, such studies were helpful to understand and to provide the big picture of PD diagnosis in GIE by considering various factors.

Table 6 summarises studies devoted to diagnosing SF_6 insulated equipment using DCA and illustrates the different factors that influence gas decomposition with key findings obtained at various PD conditions and measurement equipment. The primary decomposition components used for analysing internal deterioration under different combinations of defects are also presented.

The table also reveals that chemical detection techniques were widely adopted to diagnose the internal status of GIE under various PD conditions; mainly, GC and FTIR. Furthermore, most of the studies have considered the SF_6 decomposition under PD. The effects of gas pressure, applied voltage, ageing, and impurities such as H_2O and O_2 have also been investigated. Thus, it can be concluded that considering these factors is significant for a more comprehensive evaluation of GIS's insulation status.

B. OVERVIEW OF PD DIAGNOSIS AND FUTURE PERSPECTIVES

This review highlighted many studies on the monitoring and diagnosing of GIS insulation status. These studies included important observations on the recent advances in PD diagnosis using DCA method and AI algorithms. The applied data is diverse according to various factors and approaches used to collect it. Furthermore, most of the previous studies are based on data collected in the laboratory, which is limited by the gas chamber design used to perform the decomposition tests. Accordingly, these works need to be applied for a real-life GIS to be confirmed. More efforts are needed to consider a comprehensive analysis of PD in GIS. Therefore, the diagram shown in Figure 9 illustrates the critical factors affecting the SF_6 gas decomposition and the process of monitoring and diagnosing PD in GIS.

The diagram shows that the decomposition process is influenced by physical, chemical, and operational factors, which have been investigated previously (Table 6). Moreover, due to SF_6 decomposition process complexity, the penetration of machine learning has been considered a valuable strategy to diagnose the GIS, on top of the chemical analysis of decomposition by-products. Nevertheless, selecting an appropriate model and feature parameters is critical in the diagnostic process. Machine learning techniques and decomposition by-products are promising tools that can be applied to diagnose the internal condition of GIS, with the ability of machine learning techniques to identify boundaries of various conditions numerically. However, selected model should be generalised to avoid under and overfitting problems, and also to deal with data in terms of its dimensionality and scalability. Besides, feature parameters selection is of great importance for the performance and the accuracy of the diagnostic system.

This review was intended to provide up-to-date trends in monitoring and diagnosing GIE that uses SF_6 as an insulation medium. This study has also offered advanced techniques for detecting and evaluating the severity of PD for researchers. Moreover, it is helpful for them to conduct further research on the topic.

VIII. SUMMARY AND FUTURE WORKS

Many studies on SF_6 gas that describe the leading degradation causes, diagnostic methods, and research findings had been previously reported. Nevertheless, a further review on the SF_6 decomposition process factors, such as gas pressure, discharge energy, ageing time, insulation defects, and the presence of impurities, could be helpful. This review has revealed some trends in the diagnosis of SF_6 insulated equipment, with a special focus on the PD detection using SF_6 decomposition by-product gas analysis. The study on the SF_6 decomposition by-products has attracted many researchers' attention due to its significance and promising future for PD detection. The main findings of this review are summarised as follows:

- The positive correlation between SF_6 decomposition by-products and PD activities in a GIS promises a practical method to detect the occurrence of PD and its causes. Key by-product gases and their ratios may be used to optimise diagnosis accuracy. Furthermore, the PD severity level can also be assessed using the same technique.

- In developing the PD diagnosis technique based on SF_6 decomposition in GIS, it is paramount to consider factors such as the presence of impurities, defect configuration, gas pressure, applied voltage, and ageing time.
- Several issues were faced by many PD detection techniques. Among these are the interference faced especially for on-site applications and the limitation in by-product gas detection range. Due to limitations often faced by any single diagnosis technique, utilisation of combined techniques for PD detection in a GIS may improve the performance of the PD diagnosis and overall GIS monitoring system.
- SF_6 by-products analyses using machine learning algorithms show a promising detection approach. Nevertheless, feature's parameters and pattern recognition algorithm selection are a challenge that needs to be addressed further, especially in the presence of multiple PD sources.
- Future studies are recommended to further investigate the SF_6 gas decomposition with consideration of various factors, the results of which can be used to develop a standardised PD diagnosis technique based on SF_6 gas decomposition.

ACKNOWLEDGMENT

This research was funded by Universiti Teknologi Malaysia (05G88, 4B482, and 05G89)

REFERENCES

[1] C. H. Liu, S. Palanisamy, S. M. Chen, P. S. Wu, L. Yao, and B. S. Lou, "Mechanism of formation of SF_6 decomposition gas products and its identification by GC-MS and electrochemical methods: A mini review," *Int. J. Electrochem. Sci.*, vol. 10, no. 5, pp. 4223–4231, 2015.

[2] C. T. Dervos and P. Vassiliou, "Sulfur hexafluoride (SF_6): Global environmental effects and toxic byproduct formation," *J. Air Waste Manage. Assoc.*, vol. 50, no. 1, pp. 137–141, Jan. 2000.

[3] X. Zhang, Z. Cui, Y. Li, H. Xiao, Y. Li, and J. Tang, "Study on degradation of SF_6 in the presence of H_2O and O_2 using dielectric barrier discharge," *IEEE Access*, vol. 6, pp. 72748–72756, 2018.

[4] M. Zhao, T. Lin, X. Yan, D. Han, and G. Zhang, "Influence of trace H_2O and O_2 on SF_6 decomposition characteristics under corona discharge based on oxygen isotope tracer," *Trans. China Electrotech. Soc.*, vol. 33, no. 20, pp. 4722–4728, 2018.

[5] F. Zeng, J. Tang, X. Zhang, Q. Yao, and Y. Miao, "SF_6 partial overthermal decomposition characteristics of thermal fault in organic insulating materials," *IEEE Trans. Dielectr. Electr. Insul.*, vol. 23, no. 2, pp. 829–837, Apr. 2016.

[6] F. Zeng, S. Wu, Z. Lei, C. Li, J. Tang, Q. Yao, and Y. Miao, "SF_6 fault decomposition feature component extraction and triangle fault diagnosis method," *IEEE Trans. Dielectr. Electr. Insul.*, vol. 27, no. 2, pp. 581–589, Apr. 2020.

[7] X. Zhang, H. Liu, J. Ren, J. Li, and X. Li, "Fourier transform infrared spectroscopy quantitative analysis of SF_6 partial discharge decomposition components," *Spectrochim. Acta A, Mol. Biomol. Spectrosc.*, vol. 136, pp. 884–889, Feb. 2015.

[8] R. Sarathi and R. Umamaheswari, "Understanding the partial discharge activity generated due to particle movement in a composite insulation under AC voltages," *Int. J. Electr. Power Energy Syst.*, vol. 48, pp. 1–9, Jun. 2013.

[9] F. Zeng, J. Tang, X. Zhang, S. Zhou, C. Pan, and R. A. Sánchez, "Typical internal defects of gas-insulated switchgear and partial discharge characteristics," in *Simulation and Modelling of Electrical Insulation Weaknesses in Electrical Equipment*. Rijeka, Croatia: InTech, 2018.

[10] Z. Cao, J. Tang, F. Zeng, Q. Yao, and Y. Miao, "SF_6 positive DC partial discharge decomposition components under four typical insulation defects," *IET Gener., Transmiss. Distrib.*, vol. 13, no. 1, pp. 1–8, 2019.

[11] S. Ji, L. Zhong, Y. Wang, J. Li, Y. Cui, and W. Wang, "SF_6 decomposition of typical CT defect models," *IEEE Trans. Dielectr. Electr. Insul.*, vol. 22, no. 5, pp. 2864–2870, Oct. 2015.

[12] Y. Khan, A. A. Khan, F. N. Budiman, A. Beroual, N. H. Malik, and A. A. Al-Arainy, "Partial discharge pattern analysis using support vector machine to estimate size and position of metallic particle adhering to spacer in GIS," *Electr. Power Syst. Res.*, vol. 116, pp. 391–398, Nov. 2014.

[13] D. Evagorou, A. Kyprianou, P. L. Lewin, and A. Stavrou, "Feature extraction of partial discharge signals using the wavelet packet transform and classification with a probabilistic neural network," *IET Sci., Meas. Technol.*, vol. 4, no. 3, pp. 177–192, May 2010.

[14] A. A. Mas'ud, B. G. Stewart, and S. G. McMeekin, "An investigative study into the sensitivity of different partial discharge $\varphi - q - n$ pattern resolution sizes on statistical neural network pattern classification," *Measurement*, vol. 92, pp. 497–507, Oct. 2016.

[15] M.-S. Su, C.-C. Chia, C.-Y. Chen, and J.-F. Chen, "Classification of partial discharge events in GILBS using probabilistic neural networks and the fuzzy C-means clustering approach," *Int. J. Electr. Power Energy Syst.*, vol. 61, pp. 173–179, Oct. 2014.

[16] F. Zeng, S. Wu, X. Yang, Z. Wan, J. Tang, M. Zhang, and Q. Yao, "Fault diagnosis and condition division criterion of DC gas insulating equipment based on SF_6 partial discharge decomposition characteristics," *IEEE Access*, vol. 7, pp. 29869–29881, 2019.

[17] J. Tang, X. Rao, F. Zeng, W. Cai, L. Cheng, and C. Zhang, "Influence mechanisms of trace H_2O on the generating process of SF_6 spark discharge decomposition components," *Plasma Chem. Plasma Process.*, vol. 37, no. 1, pp. 325–340, Jan. 2017.

[18] B. Tang, Y. Sun, S. Wu, K. Gao, X. Yan, and F. Zeng, "Comprehensive evaluation and application of GIS insulation condition Part 2: Construction and application of comprehensive evaluation model considering universality and economic value," *IEEE Access*, vol. 7, pp. 129127–129135, 2019.

[19] Q. Khan, S. S. Refaat, H. Abu-Rub, and H. A. Toliyat, "Partial discharge detection and diagnosis in gas insulated switchgear: State of the art," *IEEE Elect. Insul. Mag.*, vol. 35, no. 4, pp. 16–33, Jul. 2019.

[20] V. M. Ibrahim, Z. Abdul-Malek, and N. A. Muhamad, "Status review on gas insulated switchgear partial discharge diagnostic technique for preventive maintenance," *Indonesian J. Electr. Eng. Comput. Sci.*, vol. 7, no. 1, pp. 9–17, Jul. 2017.

[21] S. Li and J. Li, "Condition monitoring and diagnosis of power equipment: Review and prospective," *High Voltage*, vol. 2, no. 2, pp. 82–91, 2017.

[22] D. Xiao, *Gas Discharge and Gas Insulation*, vol. 6. Berlin, Germany: Springer Berlin Heidelberg, 2016.

[23] S. Xiao, D. Chen, J. Tang, and Y. Li, "Adsorption behavior of γ-Al_2O_3 toward heptafluoroisobutyronitrile and its decompositions: Theoretical and experimental insights," *IEEE Access*, vol. 8, pp. 36741–36748, 2020.

[24] F. Zeng, Z. Lei, X. Yang, J. Tang, Q. Yao, and Y. Miao, "Evaluating DC partial discharge with SF_6 decomposition characteristics," *IEEE Trans. Power Del.*, vol. 34, no. 4, pp. 1383–1392, Aug. 2019.

[25] J. Tang, F. Zeng, J. Pan, X. Zhang, Q. Yao, J. He, and X. Hou, "Correlation analysis between formation process of SF_6 decomposed components and partial discharge qualities," *IEEE Trans. Dielectr. Electr. Insul.*, vol. 20, no. 3, pp. 864–875, Jun. 2013.

[26] R. J. Van Brunt and J. T. Herron, "Fundamental processes of SF_6 decomposition and oxidation in glow and corona discharges," *IEEE Trans. Elect. Insul.*, vol. 25, no. 1, pp. 75–94, Feb. 1990.

[27] R. J. van Brunt and J. T. Herron, "Plasma chemical model for decomposition of SF_6 in a negative glow corona discharge," *Phys. Scripta*, vol. 1994, T53, pp. 9–29, Jan. 1994.

[28] J. Tang, F. Liu, Q. Meng, X. Zhang, and J. Tao, "Partial discharge recognition through an analysis of SF_6 decomposition products Part 1: Decomposition characteristics of SF_6 under four different partial discharges," *IEEE Trans. Dielectr. Elect. Insul.*, vol. 19, no. 1, pp. 29–36, Feb. 2012.

[29] J. Tang, F. Zeng, X. Zhang, J. Pan, Q. Yao, X. Hou, and Y. Tang, "Relationship between decomposition gas ratios and partial discharge energy in GIS, and the influence of residual water and oxygen," *IEEE Trans. Dielectr. Electr. Insul.*, vol. 21, no. 3, pp. 1226–1234, Jun. 2014.

[30] A. Derdouri, J. Casanovas, R. Hergli, R. Grob, and J. Mathieu, "Study of the decomposition of wet SF_6, subjected to 50-Hz ac corona discharges," *J. Appl. Phys.*, vol. 65, no. 5, pp. 1852–1857, Mar. 1989.
[31] X. Xiao, H. Miao, M. Li, and B. Qi, "The two-level fault diagnosis model of SF_6 electrical equipment," in *Proc. 3rd IEEE Int. Conf. Comput. Commun. (ICCC)*, Dec. 2017, pp. 2868–2872.
[32] J. Chen, L. Li, W. Yao, Y. Tang, X. Zheng, J. Yu, Y. Luo, and W. Zhou, "Estimation of the type of low energy discharge in GIS adopting characteristic gas," *Wuhan Univ. J. Natural Sci.*, vol. 16, no. 4, pp. 319–324, Aug. 2011.
[33] F. Y. Chu, "SF_6 decomposition in gas-insulated equipment," *IEEE Trans. Electr. Insul.*, vol. EI-21, no. 5, pp. 693–725, Oct. 1986.
[34] Y. Fu, M. Rong, K. Yang, A. Yang, and X. Wang, "Calculated rate constants of the chemical reactions involving the main byproducts SO_2F, SOF_2, SO_2F_2 of SF_6 decomposition in power equipment," *J. Phys. D, Appl. Phys.*, vol. 49, no. 15, Apr. 2016, Art. no. 155502.
[35] X. Zhang, E. Gockenbach, C. Y. Wang, G. Song, and X. L. Yan, "SF_6 decomposition and fault type in SF_6 gas insulated equipment," in *Proc. Int. Conf. High Voltage Eng. Appl.*, Sep. 2012, pp. 514–517.
[36] X. Wang, Y. Fu, M. Rong, X. Li, Q. Gao, A. Yang, and D. Liu, "Investigation on the formation reactions of SOF_4 and SO_2F_2 under electric discharges," in *Proc. Int. Conf. Condition Monitor. Diagnosis (CMD)*, Sep. 2016, pp. 190–193.
[37] R. Yang, M. Xu, J. Yan, M. Yang, Y. Geng, Z. Liu, and J. Wang, "Decomposition characteristics of SF_6 under arc discharge and the effects of trace H_2O, O_2, and PTFE vapour on its by-products," *Energies*, vol. 14, no. 2, p. 414, Jan. 2021.
[38] X. Rao, J. Tang, F. Zeng, D. Li, X. Xia, Y. Su, and Y. Lu, "Mechanism of trace O_2 on SF_6 characteristic decomposed components under spark discharge," *Plasma Chem. Plasma Process.*, vol. 40, no. 2, pp. 469–481, Mar. 2020.
[39] W. Ding, G. Li, X. Ren, X. Yan, F. Li, W. Zhou, and F. Wang, "A comparison of SF_6 decomposition characteristics under corona with point-to-plane electrode defect and spark with floating potential defect," *IEEE Trans. Dielectr. Electr. Insul.*, vol. 22, no. 6, pp. 3278–3289, Dec. 2015.
[40] J. Tang, X. Rao, B. Tang, X. Liu, and X. Gong, "Investigation on SF_6 spark decomposition characteristics under different pressures," *IEEE Trans. Dielectr. Elect. Insul.*, vol. 24, no. 4, pp. 2066–2075, Sep. 2017.
[41] S. Wu, F. Zeng, J. Tang, Q. Yao, and Y. Miao, "Triangle fault diagnosis method for SF_6 gas-insulated equipment," *IEEE Trans. Power Del.*, vol. 34, no. 4, pp. 1470–1477, Aug. 2019.
[42] H. Wen and X. Zhang, "Overheating decomposition characteristics of epoxy dielectrics in SF_6 atmosphere," *IEEE Trans. Dielectr. Electr. Insul.*, vol. 26, no. 5, pp. 1411–1417, Oct. 2019.
[43] J. Wang, W. Ding, J. Yan, Y. Wang, Y. Wang, Z. Li, and G. Li, "Decomposition characteristics of SF_6 under overheating conditions," *IEEE Trans. Dielectr. Electr. Insul.*, vol. 24, no. 6, pp. 3405–3415, Dec. 2017.
[44] J. Tang, J. Pan, Q. Yao, Y. Miao, X. Huang, and F. Zeng, "Feature extraction of SF_6 thermal decomposition characteristics to diagnose overheating fault," *IET Sci., Meas. Technol.*, vol. 9, no. 6, pp. 751–757, 2015.
[45] Y. Wang, L. Li, and W. Yao, "SF_6 byproducts in high-humidity environment: An experimental evaluation between 200°C and 500°C," *J. Electromagn. Anal. Appl.*, vol. 3, no. 6, pp. 179–183, 2011.
[46] T. Li, X. Pang, B. Jia, Y. Xia, S. Zeng, H. Liu, H. Tian, F. Lin, and D. Wang, "Detection and diagnosis of defect in GIS based on X-ray digital imaging technology," *Energies*, vol. 13, no. 3, p. 661, Feb. 2020.
[47] J. K. Olthoff and R. J. Van Brunt, "Decomposition of sulfur hexafluoride by X-rays," in *Gaseous Dielectrics VII*. Boston, MA, USA: Springer, 1994, pp. 417–422.
[48] J. Wang, W. Ding, Y. Liu, Z. Zheng, and C. Ge, "Application of X-ray inspection for ultra high voltage gas-insulated switchgear," *IEEE Trans. Power Del.*, vol. 34, no. 4, pp. 1412–1422, Aug. 2019.
[49] N. C. Sahoo, M. M. A. Salama, and R. Bartnikas, "Trends in partial discharge pattern classification: A survey," *IEEE Trans. Dielectr. Elect. Insul.*, vol. 12, no. 2, pp. 248–264, Apr. 2005.
[50] J. Tang, F. Liu, Q. Meng, X. Zhang, and J. Tao, "Partial discharge recognition through an analysis of SF_6 decomposition products Part 2: Feature extraction and decision tree-based pattern recognition," *IEEE Trans. Dielectr. Electr. Insul.*, vol. 19, no. 1, pp. 37–44, Feb. 2012.
[51] T. Lin, D. Han, G. Zhang, and Y. Liu, "Formation characteristics of SF_6 decomposition under partial discharge induced by metal protrusions with varying degrees of severity," *Electr. Power Compon. Syst.*, vol. 42, no. 16, pp. 1839–1848, 2014.
[52] J. Tang, F. Liu, X. Zhang, X. Liang, and Q. Fan, "Partial discharge recognition based on SF_6 decomposition products and support vector machine," *IET Sci., Meas. Technol.*, vol. 6, no. 4, pp. 198–204, 2012.
[53] Z. Cao, J. Tang, and Y. Zhou, "SF_6 decomposition components under different metallic free-conducting wire-type particles in positive DC partial discharge," *IEEJ Trans. Elect. Electron. Eng.*, vol. 14, no. 2, pp. 214–220, Feb. 2019.
[54] Z.-C. Luo, F.-Y. Han, B. Tang, L.-F. Zhang, C.-Y. Liu, Q.-Q. Liang, L.-P. Zhu, and J.-M. Zhang, "Optical properties and decomposition mechanisms of SF_6 at different partial discharge determined by infrared spectroscopy," *AIP Adv.*, vol. 8, no. 6, Jun. 2018, Art. no. 065107.
[55] S. Kusumoto, S. Itoh, Y. Tsuchiya, H. Mukae, S. Matsuda, and K. Takahashi, "Diagnostic technique of gas insulated substation by partial discharge detection," *IEEE Trans. Power App. Syst.*, vol. PAS-99, no. 4, pp. 1456–1465, Jul. 1980.
[56] I. J. Kemp, "Partial discharge plant-monitoring technology: Present and future developments," *IEE Proc. Sci., Meas. Technol.*, vol. 142, no. 1, pp. 4–10, 1995.
[57] H. Chai, B. T. Phung, and S. Mitchell, "Application of UHF sensors in power system equipment for partial discharge detection: A review," *Sensors*, vol. 19, no. 5, p. 1029, Feb. 2019.
[58] D. Dai, X. Wang, Y. Zhao, Y. Zhang, and J. Zhang, "GIS insulation fault diagnosis based on detection of SF_6 decomposition products," in *Proc. 9th Int. Conf. Measuring Technol. Mechatronics Autom. (ICMTMA)*, Jan. 2017, pp. 60–67.
[59] L. Li, J. Tang, and Y. Liu, "Application of joint electro-chemical detection for gas insulated switchgear fault diagnosis," *J. Electr. Eng. Technol.*, vol. 10, no. 4, pp. 1765–1772, Jul. 2015.
[60] M. Ren, M. Dong, Z. Ren, H. D. Peng, and A. C. Qiu, "Transient earth voltage measurement in PD detection of artificial defect models in SF_6," *IEEE Trans. Plasma Sci.*, vol. 40, no. 8, pp. 2002–2008, Aug. 2012.
[61] A. R. Mor, L. C. C. Herdia, and F. A. Muñoz, "A novel approach for partial discharge measurements on GIS using HFCT sensors," *Sensors*, vol. 18, no. 12, p. 4482, Dec. 2018.
[62] X. Han, J. Li, L. Zhang, P. Pang, and S. Shen, "A novel PD detection technique for use in GIS based on a combination of UHF and optical sensors," *IEEE Trans. Instrum. Meas.*, vol. 68, no. 8, pp. 2890–2897, Aug. 2019.
[63] Y. Zhao, X. Wang, D. Dai, Z. Dong, and Y. Huang, "Partial discharge early-warning through ultraviolet spectroscopic detection of SO_2," *Meas. Sci. Technol.*, vol. 25, no. 3, Mar. 2014, Art. no. 035002.
[64] W. Si, J. Li, D. Li, J. Yang, and Y. Li, "Investigation of a comprehensive identification method used in acoustic detection system for GIS," *IEEE Trans. Dielectr. Electr. Insul.*, vol. 17, no. 3, pp. 721–732, Jun. 2010.
[65] H. D. Ilkhechi and M. H. Samimi, "Applications of the acoustic method in partial discharge measurement: A review," *IEEE Trans. Dielectr. Electr. Insul.*, vol. 28, no. 1, pp. 42–51, Feb. 2021.
[66] M. Ren, B. Song, T. Zhuang, and S. Yang, "Optical partial discharge diagnostic in SF_6 gas insulated system via multi-spectral detection," *ISA Trans.*, vol. 75, pp. 247–257, Apr. 2018.
[67] G.-M. Ma, H.-Y. Zhou, M. Zhang, C.-R. Li, Y. Yin, and Y.-Y. Wu, "A high sensitivity optical fiber sensor for GIS partial discharge detection," *IEEE Sensors J.*, vol. 19, no. 20, pp. 9235–9243, Oct. 15, 2019.
[68] M. Ren, J. Zhou, S. Yang, T. Zhuang, M. Dong, and R. Albarracin, "Optical partial discharge diagnosis in SF_6 gas-insulated system with SiPM-based sensor array," *IEEE Sensors J.*, vol. 18, no. 13, pp. 5532–5540, Jul. 2018.
[69] M. Ren, S. Wang, J. Zhou, T. Zhuang, and S. Yang, "Multispectral detection of partial discharge in SF_6 gas with silicon photomultiplier-based sensor array," *Sens. Actuators A, Phys.*, vol. 283, pp. 113–122, Nov. 2018.
[70] S.-Y. Wu and S.-S. Zheng, "Detection of partial discharge in GIS and transformer under impulse voltage by fluorescent optical fiber sensor," *IEEE Sensors J.*, vol. 21, no. 9, pp. 10675–10684, May 2021.
[71] V. M. Ibrahim, Z. Abdul-Malek, and N. A. Muhamad, "Chemical byproduct diagnostic technique for gas insulated switchgear condition monitoring," *Indonesian J. Elect. Eng. Comput. Sci.*, vol. 7, no. 1, pp. 18–28, 2017.
[72] Y. Han, Y. Zhang, and H. Liu, "Gas chromatography: Principles," in *Reference Module in Chemistry, Molecular Sciences and Chemical Engineering*. Amsterdam, The Netherlands: Elsevier, 2017, pp. 237–244.
[73] A. I. Ruiz-Matute, S. Rodríguez-Sánchez, M. L. Sanz, and A. C. Soria, "Chromatographic technique: Gas chromatography (GC)," in *Modern Techniques for Food Authentication*. Cambridge, MA, USA: Academic, 2018, pp. 415–458.

[74] H. M. Heise, R. Kurte, P. Fischer, D. Klockow, and P. R. Janissek, "Gas analysis by infrared spectroscopy as a tool for electrical fault diagnostics in SF_6 insulated equipment," *Fresenius J. Anal. Chem.*, vol. 358, no. 1, pp. 793–799, Mar. 1997.

[75] B. C. Smith, *Fundamentals of Fourier Transform Infrared Spectroscopy*. Boca Raton, FL, USA: CRC Press, 2011.

[76] X. Fan, L. Li, Y. Zhou, N. Tang, Z. Zou, and X. Li, "Online detection technology for SF_6 decomposition products in electrical equipment: A review," *IET Sci., Meas. Technol.*, vol. 12, no. 6, pp. 707–711, Sep. 2018.

[77] X. Zhang, J. Tang, S. Xiao, and F. Zeng, "The SF_6 decomposition mechanism: Background and significance," in *Nanomaterials Based Gas Sensors for SF_6 Decomposition Components Detection*. London, U.K.: IntechOpen, 2017.

[78] X. Zhang, L. Yu, J. Tie, and X. Dong, "Gas sensitivity and sensing mechanism studies on Au-doped TiO_2 nanotube arrays for detecting SF_6 decomposed components," *Sensors*, vol. 14, no. 10, pp. 19517–19532, Oct. 2014.

[79] A.-J. Yang, D.-W. Wang, X.-H. Wang, J.-F. Chu, P.-L. Lv, Y. Liu, and M.-Z. Rong, "Phosphorene: A promising candidate for highly sensitive and selective SF_6 decomposition gas sensors," *IEEE Electron Device Lett.*, vol. 38, no. 7, pp. 963–966, Jul. 2017.

[80] X. Zhang, X. Wu, L. Yu, B. Yang, and J. Zhou, "Highly sensitive and selective polyaniline thin-film sensors for detecting SF_6 decomposition products at room temperature," *Synth. Met.*, vol. 200, pp. 74–79, Feb. 2015.

[81] X. Zhang, J. Zhang, Y. Jia, P. Xiao, and J. Tang, "TiO_2 nanotube array sensor for detecting the SF_6 decomposition product SO_2," *Sensors*, vol. 12, no. 3, pp. 3302–3313, Mar. 2012.

[82] M. Yoshida, H. Kojima, N. Hayakawa, F. Endo, and H. Okubo, "Evaluation of UHF method for partial discharge measurement by simultaneous observation of UHF signal and current pulse waveforms," *IEEE Trans. Dielectr. Electr. Insul.*, vol. 18, no. 2, pp. 425–431, Apr. 2011.

[83] H. Janani, B. Kordi, and M. J. Jozani, "Classification of simultaneous multiple partial discharge sources based on probabilistic interpretation using a two-step logistic regression algorithm," *IEEE Trans. Dielectr. Electr. Insul.*, vol. 24, no. 1, pp. 54–65, Feb. 2017.

[84] J. Tang, F. Liu, X. Zhang, X. Ren, and M. Fan, "Characteristics of the concentration ratio of SO_2F_2 to SOF_2 as the decomposition products of SF_6 under corona discharge," *IEEE Trans. Plasma Sci.*, vol. 40, no. 1, pp. 56–62, Jan. 2012.

[85] X. Zhang, S. Tian, S. Xiao, Y. Huang, and F. Liu, "Partial discharge decomposition characteristics of typical defects in the gas chamber of SF_6 insulated ring network cabinet," *IEEE Trans. Dielectr. Electr. Insul.*, vol. 24, no. 3, pp. 1794–1801, Jun. 2017.

[86] N. A. Muhamad, I. Visa Musa, Z. Abdul Malek, and A. Salah Mahdi, "Classification of partial discharge fault sources on SF_6 insulated switchgear based on twelve by-product gases random forest pattern recognition," *IEEE Access*, vol. 8, pp. 212659–212674, 2020.

[87] L. Zhong, S. Ji, K. Liu, Q. Xiong, and L. Zhu, "Decomposition characteristics of SF_6 under three typical defects and the diagnostic application of triangle method," *IEEE Trans. Dielectr. Elect. Insul.*, vol. 23, no. 5, pp. 2594–2606, Oct. 2016.

[88] J. Tang, X. Yang, D. Yang, Q. Yao, Y. Miao, C. Zhang, and F. Zeng, "Using SF_6 decomposed component analysis for the diagnosis of partial discharge severity initiated by free metal particle defect," *Energies*, vol. 10, no. 8, p. 1119, Aug. 2017.

[89] D. Han, T. Lin, G. Zhang, Y. Liu, and Q. Yu, "SF_6 gas decomposition analysis under point-to-plane 50 Hz AC corona discharge," *IEEE Trans. Dielectr. Electr. Insul.*, vol. 22, no. 2, pp. 799–805, Apr. 2015.

[90] Y. Zhang, Y. Wang, Y. Liu, X. Dong, H. Xia, Z. Zhang, and J. Li, "Optical H_2S and SO_2 sensor based on chemical conversion and partition differential optical absorption spectroscopy," *Spectrochim. Acta A, Mol. Biomol. Spectrosc.*, vol. 210, pp. 120–125, Mar. 2019.

[91] L. Zhong, S. Ji, K. Liu, L. Zhu, and Q. Xiong, "Influence of moisture contents with a low value below 1500μL/L on SF_6 decomposition characteristics," in *Proc. IEEE Int. Power Modulator High Voltage Conf. (IPMHVC)*, Jul. 2016, pp. 315–319.

[92] R. J. Van Brunt, "Production rates for oxyfluorides SOF_2, SO_2F_2, and SOF_4 in SF_6 corona discharges," *J. Res. Nat. Bureau Standards*, vol. 90, no. 3, pp. 229–253, 1985.

[93] F. Zeng, J. Tang, H. Sun, J. Pan, Q. Yao, J. He, and X. Hou, "Quantitative analysis of the influence of regularity of SF_6 decomposition characteristics with trace O_2 under partial discharge," *IEEE Trans. Dielectr. Electr. Insul.*, vol. 21, no. 4, pp. 1462–1470, Aug. 2014.

[94] L. Kai, J. Shengchang, Z. Lipeng, and Z. Lingyu, "The mechanism of SF_6 decomposition characteristics under partial discharge at different gas pressures and voltage," in *Proc. Int. Conf. Condition Monitor. Diagnosis (CMD)*, Xi'an, China, Sep. 2016, pp. 578–581.

[95] Y. Wang, S. Ji, Q. Zhang, J. Ren, J. Li, and W. Wang, "Experimental investigations on low-energy discharge in SF_6 under low-moisture conditions," *IEEE Trans. Plasma Sci.*, vol. 42, no. 2, pp. 307–314, Feb. 2014.

[96] L. Zhong, F. Wang, S. Chen, Q. Sun, J. Liu, S. Ji, and K. Liu, "Influence mechanism of pressure on SF_6 decomposition characteristics under AC corona discharge," *IEEE Trans. Dielectr. Electr. Insul.*, vol. 26, no. 6, pp. 1989–1997, Dec. 2019.

[97] F. Liu, J. Tang, and Y. Liu, "Mathematical model of influence of oxygen and moisture on feature concentration ratios of SF_6 decomposition products," in *Proc. IEEE Power Energy Soc. Gen. Meeting*, Jul. 2012, pp. 1–5.

[98] T. Lin, D. Han, G. Zhang, and D. Liu, "Influence of trace O_2 on SF_6 decomposition characteristics under partial discharge based on oxygen isotope tracer," *IEEE Trans. Dielectr. Electr. Insul.*, vol. 24, no. 3, pp. 1600–1607, Jun. 2017.

[99] X. Pang, H. Wu, J. Pan, Y. Qi, X. Li, J. Zhang, and Q. Xie, "Analysis of correlation between internal discharge in GIS and SF_6 decomposition products," in *Proc. IEEE Int. Conf. High Voltage Eng. Appl. (ICHVE)*, Sep. 2018, pp. 1–4.

[100] W. Zhou, Y. Zheng, S. Yang, H. Li, B. Wang, and S. Qiao, "Detection of intense partial discharge of epoxy insulation in SF_6 insulated equipment using carbonyl sulfide," *IEEE Trans. Dielectr. Electr. Insul.*, vol. 23, no. 5, pp. 2942–2948, Oct. 2016.

[101] F. Zeng, J. Tang, X. Zhang, J. Pan, Q. Yao, and X. Hou, "Influence regularity of trace H_2O on SF_6 decomposition characteristics under partial discharge of needle-plate electrode," *IEEE Trans. Dielectr. Electr. Insul.*, vol. 22, no. 1, pp. 287–295, Feb. 2015.

[102] J. Tang, J. Pan, X. Zhang, F. Zeng, Q. Yao, and X. Hou, "Correlation analysis between SF_6 decomposed components and charge magnitude of partial discharges initiated by free metal particles," *IET Sci., Meas. Technol.*, vol. 8, no. 4, pp. 170–177, 2014.

[103] T. Lin, D. Han, X. Jin, and G. Q. Zhang, "Experimental study for SF_6 decomposition byproducts formation mechanisms in 50 Hz AC corona discharge and flashover," in *Proc. Annu. Rep. Conf. Electr. Insul. Dielectric Phenomena*, Oct. 2013, pp. 1221–1224.

[104] Z. Cao, Y. Bai, Y. Zhou, G. Wei, Y. Zhang, and J. Wang, "An investigation of negative DC partial discharge decomposition of SF_6 under different metal materials," *IEEE Access*, vol. 8, pp. 35105–35112, 2020.

[105] J. Tang, D. Yang, F. Zeng, B. Tang, and K. Li, "Correlation characteristics between gas pressure and SF_6 decomposition under negative DC partial discharge," *IET Gener., Transmiss. Distrib.*, vol. 12, no. 5, pp. 1240–1246, Mar. 2018.

AMMAR SALAH MAHDI received the bachelor's degree in electrical engineering from the University of Basrah, Iraq, in 2009, and the master's degree in electrical engineering from Universiti Tun Hussein Onn Malaysia (UTHM), in 2019. He is currently pursuing the Ph.D. degree with the Institute of High Voltage and High Current (IVAT), Universiti Teknologi Malaysia (UTM). His research interest includes pattern recognition for GIS status under partial discharge fault.

ZULKURNAIN ABDUL-MALEK (Senior Member, IEEE) received the B.E. degree from Monash University, Melbourne, Australia, in 1989, and the M.Sc. degree in electrical and electromagnetic engineering with industrial applications and the Ph.D. degree in high-voltage engineering from Cardiff University, in 1995 and 1999, respectively. He has been with Universiti Teknologi Malaysia, for 31 years, where he is currently a Professor and the Director of the Institute of High Voltage and High Current. He has published more than 150 papers in various technical journals and conference proceedings. His research interests include surge arrester intelligent condition monitoring, lightning-related EMC, warning systems, lightning protection systems, electrical discharge, condition monitoring, and nanodielectrics. He is actively involved in many national and international committees.

RAI NAVEED ARSHAD received the M.Sc. degree in electronics from Quaid-I-Azam University, Islamabad, the M.S. degree in systems engineering from the Pakistan Institute of Engineering and Applied Sciences (PIEAS), Islamabad, and the Ph.D. degree in electrical engineering from Universiti Teknologi Malaysia (UTM), Johor, Malaysia. His research interests include power electronics, high-voltage engineering, pulsed power technology, food technologies, and non-thermal processing. He is also developing an electroporator for liquid food treatment.